

Massive black hole remnants of the first stars I: abundance in present-day galactic haloes

Ranty R. Islam[†], James E. Taylor and Joseph Silk

Astrophysics, Denys Wilkinson Building, Keble Road, Oxford, OX1 3RH, UK

arXiv:astro-ph/0307171v1 9 Jul 2003

Received ...; accepted ...

ABSTRACT

We investigate the possibility that present-day galaxies and their dark matter haloes contain a population of massive black holes (MBHs) that form by hierarchical merging of the black hole remnants of the first stars in the Universe. Some of the MBHs may be large enough or close enough to the centre of the galactic host that they merge within a Hubble time. We estimate to what extent this process could contribute to the mass of the super-massive black holes (SMBHs) observed in galactic centres today. The relation between SMBH and galactic bulge mass in our model displays the same slope as that found in observations. Many MBHs will not reach the centre of the host halo, however, but continue to orbit within it. In doing so MBHs may remain associated with remnants of the satellite halo systems of which they were previously a part. Using a semi-analytical approach that explicitly accounts for dynamical friction, tidal disruption and encounters with galactic disks, we follow the hierarchical merging of MBH systems and their subsequent dynamical evolution inside the respective host haloes. In this context two types of dynamical process are examined in more detail. We predict the mass and abundance of MBHs in present-day galactic haloes, and also estimate the MBH mass accretion rates as well as bolometric luminosities for two different accretion scenarios. MBHs that have not undergone recent merging will retain associated dark matter cusps that were enhanced by black hole accretion growth, and may be possible sources of gamma rays via neutralino annihilations.

Key words: galaxies: formation – galaxies: haloes – galaxies: nuclei – cosmology: theory

1 INTRODUCTION

The presence of super-massive black holes (SMBHs) at the centres of most galaxies appears by now to be firmly established. SMBHs have estimated masses in the range $10^6 - 10^9 M_\odot$ and a number of correlations have been observed between the mass of SMBHs and properties of the galactic bulge hosting them. The first of these to be established were correlations between the mass of the SMBH, M_{smbh} and the mass or luminosity of the galactic bulge, M_{bulge} and L_{bulge} respectively (Magorrian et al. 1998; Kormendy & Gebhardt 2001; Laor 2001). More recently, a tighter correlation was found between M_{smbh} and the bulge velocity dispersion, σ_{bulge} (Gebhardt et al. 2000; Merritt & Ferrarese 2001), and also between M_{smbh} and the bulge's light profile, as parameterised by a shape index, n (Graham et al. 2001).

Since these correlations extend well beyond the direct dynamical influence of the SMBH it seems likely that there is a close link between the formation of SMBHs and the formation of their host galaxy. A recent analysis finds

that the masses of SMBHs appear to be correlated with the host circular velocity even beyond the optical radius (Ferrarese 2002). If confirmed, this implies that the SMBHs are linked to properties of the host dark matter halo. This would be the strongest hint yet that there must be a hierarchical merging component to the growth of SMBHs, since the properties of haloes are primarily determined in the context of their hierarchical build up.

Most models put forward to account for the correlations assume a close link between galaxy and SMBH formation as a starting point. We can distinguish two generic types of models. One proposes that the SMBH mass increases mainly by the merging of smaller precursors. This requires SMBH precursors to have been present in galaxies from very early on (Madau & Rees 2001; Menou, Haiman & Narayan 2001; Schneider et al. 2002). It might allow the observed correlations to be set up over a long period of time with a potentially large number of mergers through the dynamical interactions between the merging galaxies and SMBH precursors.

Another mechanism considered is growth mainly by gas

accretion within the host bulge. In this case a strong non-gravitational interaction between the growing SMBH and the bulge is required. An example of this is the radiative feedback of an accreting SMBH that changes the gas dynamics in the bulge so as to effectively control its own gas supply and establish a relation between M_{smbh} and σ_{bulge} (Silk & Rees 1998). A similar route is followed by models that tie M_{smbh} to the amount and properties of gas in the bulge (Adams, Graff & Richstone 2001). A combination of both approaches is used in the model by Haehnelt & Kauffmann (2000).

As an example of the merger-only scenario it has been shown that the merging of the massive black hole (MBH) remnants of the first stars in the Universe could account for the inferred overall abundance of SMBHs today (Schneider et al. 2002).

Here we explore this idea further to determine an upper limit on the mass to which SMBHs can grow through mergers of lower mass precursors and more importantly what the implications are for the presence of a remnant population of lower mass MBHs in the galactic halo. In doing so we assume efficient merging between MBHs, but we also consider the effect of relaxing this assumption. As the ‘seeds’ in the merging hierarchy, we consider massive black holes (MBHs) of some mass M_{seed} that are remnants of the first stars in the Universe, forming within high density peaks at redshifts of $z \sim 20-30$. We use Monte Carlo merger trees to describe the merging of haloes and then follow the dynamical evolution of merged/accreted satellite haloes and their central MBHs within larger hosts, explicitly accounting for dynamical friction, tidal stripping and disk encounters. A key prediction is that $\sim 10^3$ MBHs in the mass range $1-1000 \times M_{seed}$ should be present within the galactic halo today as a result of this process.

In a previous paper (Islam, Taylor & Silk 2003) we looked at the case of $260 M_{\odot}$ seed MBHs forming within 3σ peaks at redshift $z \sim 24$. In this paper we extend our investigation to consider four different sets of initial conditions as shown in table 1 and also compute the accretion rates of resulting MBHs in present-day haloes. The latter is used to determine the bolometric accretion luminosities. In a subsequent paper we use specific spectral models to predict optical and X-ray luminosity functions for the accreting halo MBHs. Throughout we work with a Λ CDM cosmology, specified by $\Omega_m = 0.3, \Omega_b = 0.02h^{-2}, \Omega_{\Lambda} = 0.7, h = 0.7, \sigma_8 = 0.9$.

The structure of this paper is as follows. In section 2 we briefly describe how MBHs could form as a result of the formation and evolution of the first stars in the Universe. We also introduce the semi-analytical scheme used to track the subsequent merging and dynamical evolution of MBHs. In section 3 we present the resulting distribution of MBHs in galactic haloes today. We also discuss the MBH accretion rates and to what extent these MBHs could have contributed to the mass of the SMBHs in galactic centres. In section 4 we estimate the bolometric luminosities of accreting MBHs. This should give some indication of the expected actual observable signatures. A summary of our findings and conclusion is given in section 5.

2 FORMATION AND HIERARCHICAL MERGING OF SEED MASS MBHS

2.1 Primordial star formation and MBHs

A number of recent semi-analytical (Hutching et al. 2002; Fuller & Couchman 2000; Tegmark et al. 1997) and numerical investigations (Bromm, Coppi & Larson 2002; Abel, Bryan & Norman 2000) suggest that the first stars in the Universe were likely created inside molecular clouds that fragmented out of the first baryonic cores inside dark matter haloes at very high redshifts. For common Λ CDM cosmologies in particular these *minihaloes* are found to have a mass $M_{min} \sim 10^5 - 10^6 h^{-1} M_{\odot}$ and to have collapsed at redshift $z \sim 20 - 30$. In linear collapse theory this corresponds to collapse from $2.5 - 3.5\sigma$ peaks in the initial matter density field. For instance minihaloes collapse from 3σ peaks at a redshift of about 25. This is because the mass contained in overdensities corresponding to 3σ peaks at this redshift is just above both the cosmological Jeans mass and the cooling mass¹. Cooling nevertheless proceeds much more slowly than at present; as stars have yet to form, metals that could facilitate more efficient cooling are essentially not present. This implies that even though fragmentation occurs, fragments will be much larger than in a corresponding situation today. Seed masses within these fragments can in principle accrete large amounts of matter from the cloud without further fragmentation occurring, which could eventually lead to the formation of a proto-star. (Bromm, Coppi & Larson 2002; Machacek, Bryan & Abel 2001; Omukai & Palla 2001). Only radiation pressure from the proto-star on the infalling layers of material could halt accretion and so limit the mass of the star. However, in the absence of dust the infalling matter has too low an opacity for radiation pressure to be significant (Ripamonti et al. 2002). In these stars the role of winds that could lead to significant mass loss in population I stars, is also negligible. As a result this will likely lead to the creation of very massive stars, potentially as heavy as $10^3 M_{\odot}$. These are also referred to as population III stars.

As yet nothing definite is known about the initial mass function (IMF) of these stars. However, their large mass will see many of them ending up as black holes of essentially the same mass - gravity is so strong that not even ejecta of a final supernova can escape (Heger et al. 2002).

Here we assume that in each dark matter halo forming at $z \gtrsim 20$ with a mass larger than the cooling mass, one MBH forms as the end result of any primordial star formation occurring inside the halo. These MBHs then represent the seeds for the subsequent merging process.

For our computations we have considered three different formation redshifts of minihaloes and seed MBH masses as summed up in table 1. Our choice of a seed MBH mass of $260 M_{\odot}$ is motivated by the result of Heger (2002) that massive stars above this mass will not experience a supernova at

¹ At or above the cooling mass the corresponding virial temperature, to which the baryons are heated, is high enough for cooling to proceed on a time scale that is smaller than the gravitational infall time scale. The latter is the necessary condition for fragmentation to occur.

Table 1. Masses of seed MBHs and heights of peaks in initial density field within which they formed.

	$M_{\bullet,seed}$	peak height ν_{pk}	$z_{collapse}$
A	$260 M_{\odot}$	3.0	24.6
B	$1300 M_{\odot}$	3.0	24.6
C	$260 M_{\odot}$	2.5	19.8
D	$260 M_{\odot}$	3.5	29.4

the end of their lives but will collapse directly to a MBH of essentially the same mass.

2.2 Hierarchical merging and dynamical evolution of MBHs

While the basic properties of the seed MBHs are determined by the physics of the first baryonic objects, as outlined above, the extent to which they merge to form the present-day SMBH depends on their subsequent dynamical evolution after their respective host haloes have merged. To track this evolution we use a semi-analytical code (Taylor & Babul 2001 and 2003) that combines a Monte-Carlo algorithm to generate halo merger trees with analytical descriptions for the main dynamical processes – dynamical friction, tidal stripping, and tidal heating – that determine the evolution of merged remnants within a galaxy halo.

Starting with a halo of a specific mass at the present-day, we trace the merger history of the system back to a redshift of 30, using the algorithm of Somerville & Kolatt (1999). Computational considerations limit the mass resolution of the tree to $\simeq 3 \times 10^{-5}$ of the total mass; below this limit we do not trace the merger history fully. For the more massive haloes, this resolution limit is larger than M_{min} and many of the branchings of the merger tree drop below the mass resolution limit before they reach the minihalo collapse redshift (e.g. $z = 24$ for collapse from 3σ peaks), so that we cannot always track the formation of individual black holes. To overcome this problem, if systems over M_{min} appear in the merger tree after primordial black holes have started forming at the collapse redshift, we determine how likely they are to contain one or more primordial black holes, based on the frequency of peaks of corresponding height, and populate them accordingly. In the most massive trees, haloes at the resolution limit are likely to contain several primordial black holes. In this case, we assume the black holes have merged to form a single object, in keeping with the assumption of efficient merging discussed below.

Within the merger trees, we then follow the dynamical evolution of black holes forward in time to the present-day, using the analytic model of satellite dynamics developed in Taylor & Babul (2001). Merging subhaloes are placed on realistic orbits at the virial radius of the main system, and experience dynamical friction, mass loss and heating as they move through their orbits. The background potential is modelled by a smooth Moore profile, $\rho \propto r^{-1.5} (r_s^{-1.5} + r^{-1.5})$ (Moore et al. 1999), which grows in mass according to its merger history, and changes in concentration following the relations proposed by Eke, Navarro & Steinmetz (2001). We give this profile a constant-density core of radius $0.1r_s$, to

account for the possible effects of galaxy formation in disrupting the dense central cusp.

Within this potential, the formation of a central galaxy with a disk and a spheroidal component is modelled schematically, by assuming that a third of the gas within the halo cools on the dynamical time-scale to form a galactic disk, and that major mergers disrupt this disk and transform it into a spheroid with some overall efficiency. We choose as the disruption criterion that the disk collide with an infalling satellite of mass equal to or greater than its own, and set the efficiency with which disk material is then transferred to the spheroid to 0.25. This choice of parameters is required to limit the formation of spheroids and thus produce a reasonable range of morphologies in isolated present-day $10^{12} M_{\odot}$ systems, as discussed in Taylor & Babul (2002). We do not expect the results for halo back holes to depend strongly on these parameters, although they may have some effect on the properties of the central black holes. Finally, the evolution of haloes in side branches of the merger tree is followed more approximately, by assuming that higher-order substructure (that is subhaloes within subhaloes) merges over a few dynamical times, causing its black hole component to merge as well, while unmerged substructure percolates down to a lower level in the tree. We will discuss the details of this model elsewhere (Taylor & Babul 2003); here it serves only as a backdrop for the dynamical calculations of black hole evolution.

The semi-analytic code tracks the positions of all the primordial black holes that merge with the main system and the amount of residual dark matter from their original halo that still surrounds them, if any. We classify systems as ‘naked’ if their surrounding subhalo has been completely stripped by tidal forces, and ‘normal’ otherwise. Our orbital calculations cannot follow the evolution of systems down to arbitrarily small radii within the main potential, so if black holes come within 1% of the virial radius of the centre of the potential (roughly 3 kpc for a system like the present-day Milk Way), we assume they have ‘fallen in’ and stop tracking their orbits. Black holes contained in satellites which disrupt the disk in major mergers are also assumed to fall into the centre of the potential during its subsequent rearrangement. Clearly, this assumes that black hole merging in the centre of the main system is completely efficient, so it will produce a conservative upper limit on how many black holes merge with the central SMBH. We discuss the effect of relaxing these assumptions below.

Using the semi-analytic code, we generate sets of different realisations for final halo masses of 1.6×10^{10} , 1.6×10^{11} , 1.6×10^{12} and $1.6 \times 10^{13} M_{\odot}$ for the four sets of initial conditions given in table 1.

2.3 MBH merger efficiency

Up to now we have considered any MBH as having merged with the central MBH, when it comes within one per cent (hereafter referred to as the merger region) of the virial radius of the host halo at that time. There are various ways in which the actual merger efficiency could be lower than this, and so our results above only provide an upper limit on how much the MBH merger process can contribute to the mass of central and halo MBHs.

One major source of inefficiency is of course the time it

takes for any MBH to spiral into another, and typically more massive MBH at the centre of their common host and how likely it is then for the two to merge. One does not necessarily imply the other – at early times haloes are smaller, that is, at the first encounter, the two central MBHs within any two haloes will start out much closer and so are more likely to spiral to the common centre of the halo merger remnant in a relatively short time. Because there are more low mass haloes, this might then give rise to configurations consisting of more than two MBHs and thus the possibility of sling-shot ejections. In other words some fraction of MBHs, although having travelled to the centre quickly, might eventually end up being expelled rather than merging. This has implications for the most massive trees. Haloes at the resolution limit in these trees have a mass above M_{min} and therefore might appear in the tree with several seed MBHs which we have thus far assumed to have merged to form one MBH (c.f. section 3.2). This may no longer be the case if slingshot ejections occur. Assuming that in this case the lightest MBHs are ejected, however, this should not significantly reduce the mass of the central MBH.

The assumption that MBHs within a kpc or so from the host centre merge efficiently can be used to determine an upper limit on the mass of central SMBHs. Although MBH merging may proceed much less efficiently, a number of processes could lead to rapid merging of MBHs in the galactic context.

If the mass of only the MBHs is considered, their orbital decay time scale in the host can be longer than a Hubble time. However, MBHs typically remain associated with matter from their original satellite, which increases their effective mass by a factor of at least 100 to 1000 and lowers the orbital decay time scale accordingly, allowing even relatively light MBHs ($M_{\bullet} \geq 10^3 M_{\odot}$) to spiral into the host central region (\lesssim kpc) within a Hubble time (Yu & Tremaine 2002). This is true even if the satellite itself may have actually lost most of its mass (\gtrsim 99 percent) due to tidal stripping inside the host halo and is thus classified as ‘naked’ in our treatment. This implies that only at high redshifts could seed mass MBHs have travelled to the host centre, since they would have then entered the correspondingly smaller host halo at smaller distances from the centre.

It seems then that dynamical friction can deliver MBHs to the host central regions efficiently where they then form binaries with any MBH already at the centre. The evolution of a MBH binary system in stellar background has been studied extensively (Begelman, Blandford & Rees 1980; Quinlan 1996; Milosavljević & Merritt 2001; Yu & Tremaine 2002) and the ‘hardening’ stage of binary evolution has been singled out as the ‘bottle neck’ on the way to the final merger (Milosavljević & Merritt 2001; Yu & Tremaine 2002). With dynamical friction no longer significant and orbital decay due to gravitational wave emission not yet important, one way for the binary MBHs to reduce their orbital radius is by interaction with stars in their vicinity, which can take significantly longer than a Hubble time. However, Merritt & Poon (2003) showed recently that if the galactic potential around a binary SMBH at its centre is non-axisymmetric and the stellar orbits are chaotic, the interaction rates can be larger by orders of magnitude. In principle this argument should also hold for MBHs in their respective satellites. In

fact, due to the higher number of major mergers at early times the potentials of the (mini) galaxies hosting central MBHs are much more likely to be non-axisymmetric.

However, even in the case that binary decay through interactions with stars takes prohibitively long, the presence of gas may be of crucial importance in this context (Milosavljević & Merritt 2001). High densities of gas between the binary MBHs could allow for a much faster evolution and eventual merger of the binary. Several scenarios have been suggested for this, such as a massive gas disk around the binary (Gould & Rix 2000; Armitage & Natarajan 2002) or massive gas inflow (see e.g. Begelman, Blandford & Rees 1980) in the wake of major mergers. Hydrodynamical simulations of galaxy mergers, for instance, find that up to 60 per cent of the total gas mass of two merging Milky Way-size galaxies can end up within a region only a few hundred parsecs across, which is about half the bulge scale radius (Barnes & Hernquist 1996; Naab & Burkert 2001; Barnes 2002).

Here we assume that during major mergers the gas infall will actually lead to all MBHs binaries merging. We also neglect the possibility of triple BH interactions and slingshot ejections.

3 MBHS IN PRESENT-DAY GALACTIC HALOES

A fundamental prediction of the hierarchical merging of MBHs is the existence of MBHs throughout galaxies and their haloes. Other MBHs may have already travelled to the centre and merged there to help build up the central SMBH we see in galactic centres today. In this section we determine the number, mass, accretion rates and bolometric accretion luminosities for halo MBHs and the mass of the central (S)MBH.

3.1 Abundance and Mass of MBHs in galactic haloes

3.1.1 Abundance of MBHs in galactic haloes

In figure 1 we show the abundance of all MBHs for models A, C and D and for all final halo masses. Model B, which only differs from model A by its different MBH seed mass is considered below.

In addition the total number of MBHs in the halo is given in table 2. For Milky Way sized haloes (i.e. corresponding to a final halo mass of $1.6 \times 10^{12} M_{\odot}$), for instance, we would expect between 900 to 2100 MBHs to orbit within the galactic halo depending on the model.

Here, as in all other plots of average abundances and luminosities, we have stated the standard deviation rather than the error on the ‘mean’ as a measure of the uncertainty of our results.

We found that the number of MBHs in the galactic disk out to about two disk scale radii is less than 0.2 per cent of the total number of MBHs for all final halo masses. Part of the reason for this low number is that a lot of the MBHs in the disk are orbiting at small distances of less than 1 per cent of the host virial radius and are therefore counted as having fallen to the centre since their dynamics cannot be

Table 2. Number of MBHs in halo averaged over thirty trees with associated standard deviation. We have shown the total number as well as the number in the bulge within two bulge scale radii and in the disk within two disk scale lengths and scale heights.

Halo mass	model A	model B	model C	model D
total # MBHs in halo				
1.6×10^{10}	100 ± 17	76 ± 13	170 ± 38	20 ± 6
1.6×10^{11}	640 ± 110	570 ± 120	710 ± 76	140 ± 24
1.6×10^{12}	2090 ± 360	1750 ± 170	2430 ± 550	910 ± 220
1.6×10^{13}	2130 ± 230	2250 ± 490	2200 ± 530	1970 ± 210
# MBHs in bulge				
1.6×10^{10}	0	0	0	0
1.6×10^{11}	2.3 ± 1.7	2.3 ± 1.9	4.1 ± 2.6	0.5 ± 0.7
1.6×10^{12}	36 ± 17	35 ± 13	36 ± 11	11 ± 6
1.6×10^{13}	93 ± 30	72 ± 25	77 ± 26	81 ± 29
# MBHs in disk				
1.6×10^{10}	0	0	0	0
1.6×10^{11}	0.9 ± 1.1	1.1 ± 1.2	2.3 ± 1.8	0.3 ± 0.6
1.6×10^{12}	9.3 ± 5.2	9.2 ± 4	9.2 ± 3.5	3.2 ± 2
1.6×10^{13}	14.6 ± 6.6	10.3 ± 4.3	12.6 ± 4.8	11.7 ± 5

traced accurately any more as mentioned above. Conversely the high mass end implies that apart from the central SMBH there will be one or two other MBH of about a tenth of its mass orbiting in the halo

While the mass functions display a uniform slope of $N_\bullet \propto M_\bullet^{-1}$ it is interesting to note that particularly in model A and C the mass function of MBHs in the most massive halo displays a downward departure from a power law for MBH masses less than about $M_\bullet \sim 3 \times 10^3 - 10^4 M_\odot$. As a result the total number of MBHs in the most massive halo is less than expected and is actually quite similar to that in the second most massive halo in models A and C. This is due to the mass resolution limit of the semi-analytical code as explained in section 2.2. For the most massive final haloes this limit is larger and consequently more haloes entering the hierarchy at this limit may already contain more than one seed MBHs, which we then assume have merged. The latter means that the number of MBHs with the original seed mass is reduced.

In figure 2 we show the average MBH abundance including that of naked MBHs within the virial radius of the 1.6×10^{12} and $1.6 \times 10^{10} M_\odot$ respectively for models A and B.

Compared to the mass of the bulge, disk and halo the seed MBH masses are small and so we would not expect them to significantly affect the evolution of substructure within the host. For this reason we find that, except for the high mass end, the MBH mass functions for the two different MBH seed masses are essentially the same but are offset from one another along the ordinate (representing the actual MBH mass) by a constant factor that is more or less equal to the ratio of the initial seed MBH masses. Based on this, the line bounding the grey shaded area in figure 2 represents the inferred mass function for a seed MBH with

a mass of $1.3 \times 10^4 M_\odot$, that is the case where the entire baryonic mass of an minihalo collapses into the black hole.

For a final halo mass of $1.6 \times 10^{12} M_\odot$ in both model A and B we can deduce from figure 2 that the number N of remnant MBHs in the halo follows a power law

$$N_\bullet \propto M_\bullet^{-1.01 \pm 0.04}$$

which is also the basis on which we have determined the line bounding the prohibited region for any MBH mass function. It is difficult to establish a similar uniform power law for haloes lighter than this. In this case not as many massive MBHs have formed and the shape of the MBH mass function is thus dominated at the low mass end (near the MBH seed mass) by the discrete nature of the MBH mass increase.

Figure 3 shows the number of MBHs as a function of distance from the host centre for model A only. We have also plotted the contribution of MBHs more massive than 10^4 and $10^5 M_\odot$. In addition the plot shows the fraction of naked MBHs for all of the above cases. As expected there are more naked MBHs near the centre where the steeper host gravitational potential results in stronger tidal forces that strip away more matter from any satellite present there. In all cases shown the contribution of naked MBHs typically becomes dominant at distances of less than a few percent of the host virial radius. With increasing halo mass the relative contribution of naked MBHs at small radii decreases. A reason for this is that in small haloes the tidal gradient is relatively steeper and MBHs are therefore more likely to be stripped. For the different MBH mass cuts, however, there does not appear to be any significant difference in the relative radial distribution of naked MBHs.

In figure 4 we have shown the cumulative abundance of MBHs below a given distance from the halo centre. The distribution is scaled to the virial radii of the respective haloes and results are shown for models A,C & D. What this shows

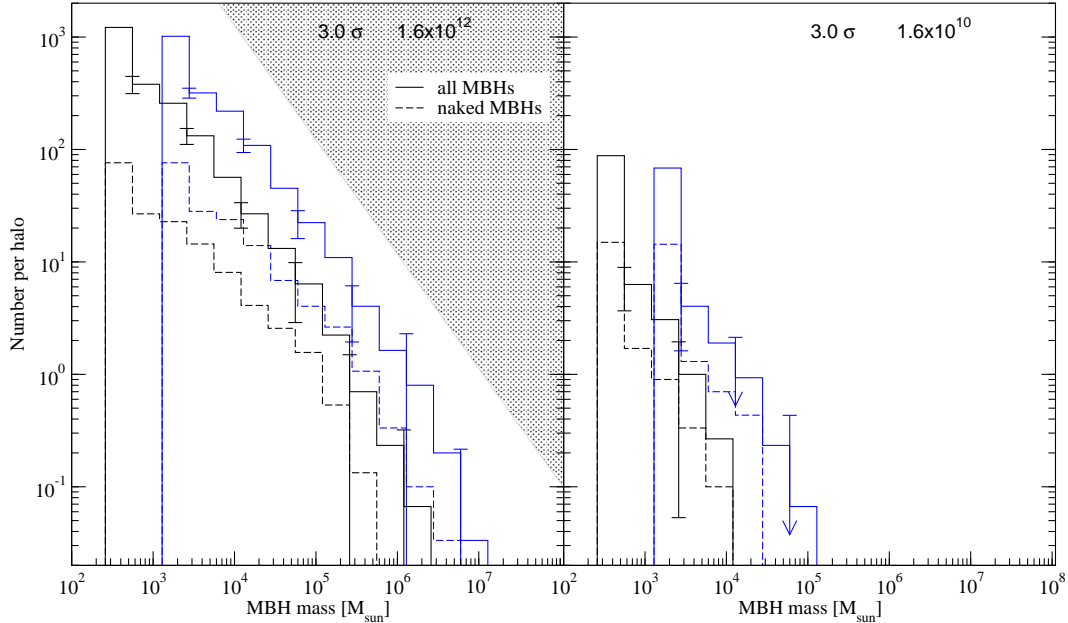


Figure 2. Comparison of models A and B: Abundance of all and naked MBHs in galactic haloes of mass $1.6 \times 10^{12} M_{\odot}$ (left panel) and $1.6 \times 10^{10} M_{\odot}$ (right). The set of curves to the left and right within each panel are for seed MBH masses of 260 and $1300 M_{\odot}$ respectively. Provided the shape of the mass function remains the same for different MBH seed masses, the shaded area in the left panel indicates the prohibited regime where seed MBHs would need to be more massive than the total amount of baryons available in the original minihalo within which they formed.

Table 3. Total mass in halo MBHs and mass of central SMBH for all final halo masses and all models. The total mass in MBHs is typically 2 – 3 times larger than the mass of the central SMBH.

	Halo mass		
	1.6×10^{10}	1.6×10^{11}	1.6×10^{12}
model A	$\sum M_{MBH}[M_{\odot}]$	$(3.4 \pm 0.59) \times 10^4$	$(3.8 \pm 0.62) \times 10^5$
	$M_{SMBH}[M_{\odot}]$	$(1.55 \pm 0.67) \times 10^4$	$(1.85 \pm 0.63) \times 10^5$
model B	$\sum M_{MBH}[M_{\odot}]$	$(1.34 \pm 0.36) \times 10^5$	$(1.68 \pm 0.32) \times 10^6$
	$M_{SMBH}[M_{\odot}]$	$(7.36 \pm 3.36) \times 10^4$	$(8.83 \pm 3.34) \times 10^5$
model C	$\sum M_{MBH}[M_{\odot}]$	$(6.48 \pm 0.98) \times 10^4$	$(4.79 \pm 1.49) \times 10^5$
	$M_{SMBH}[M_{\odot}]$	$(2.84 \pm 0.9) \times 10^4$	$(3.62 \pm 1.5) \times 10^5$
model D	$\sum M_{MBH}[M_{\odot}]$	$(5.75 \pm 1.84) \times 10^3$	$(5.63 \pm 0.99) \times 10^4$
	$M_{SMBH}[M_{\odot}]$	$(3.16 \pm 1.48) \times 10^3$	$(3.34 \pm 1.32) \times 10^4$
<hr/>			
model A	$\sum M_{MBH}[M_{\odot}]$	$(3.17 \pm 0.76) \times 10^6$	$(3.42 \pm 0.78) \times 10^7$
	$M_{SMBH}[M_{\odot}]$	$(1.5 \pm 0.64) \times 10^6$	$(1.14 \pm 0.29) \times 10^7$
model B	$\sum M_{MBH}[M_{\odot}]$	$(1.27 \pm 0.4) \times 10^7$	$(1.78 \pm 0.31) \times 10^8$
	$M_{SMBH}[M_{\odot}]$	$(6.93 \pm 2.81) \times 10^6$	$(7.42 \pm 2.93) \times 10^7$
model C	$\sum M_{MBH}[M_{\odot}]$	$(7.59 \pm 1.04) \times 10^6$	$(7.00 \pm 1.27) \times 10^7$
	$M_{SMBH}[M_{\odot}]$	$(3.23 \pm 1.21) \times 10^6$	$(2.96 \pm 1.29) \times 10^7$
model D	$\sum M_{MBH}[M_{\odot}]$	$(6.24 \pm 0.97) \times 10^5$	$(4.9 \pm 1.08) \times 10^6$
	$M_{SMBH}[M_{\odot}]$	$(2.57 \pm 1.06) \times 10^5$	$(2.33 \pm 1.33) \times 10^6$

us is that the shape of the radial distribution is fundamentally the same in all cases except for the normalisation. The latter corresponds to the difference in the total MBH abundance as shown in figure 1. We also note that, while different in all other cases, the radial distribution of MBHs are very similar again for final halo masses of 1.6×10^{12} and 1.6×10^{13}

M_{\odot} in models A and C. This is for the same reasons given above in respect of the corresponding mass functions.

An important result that emerges from both figures 1 and 4 is that both the shape of the mass abundance as well as the radial distribution of MBHs in haloes is very similar. The different normalisation of the number of and mass in MBHs

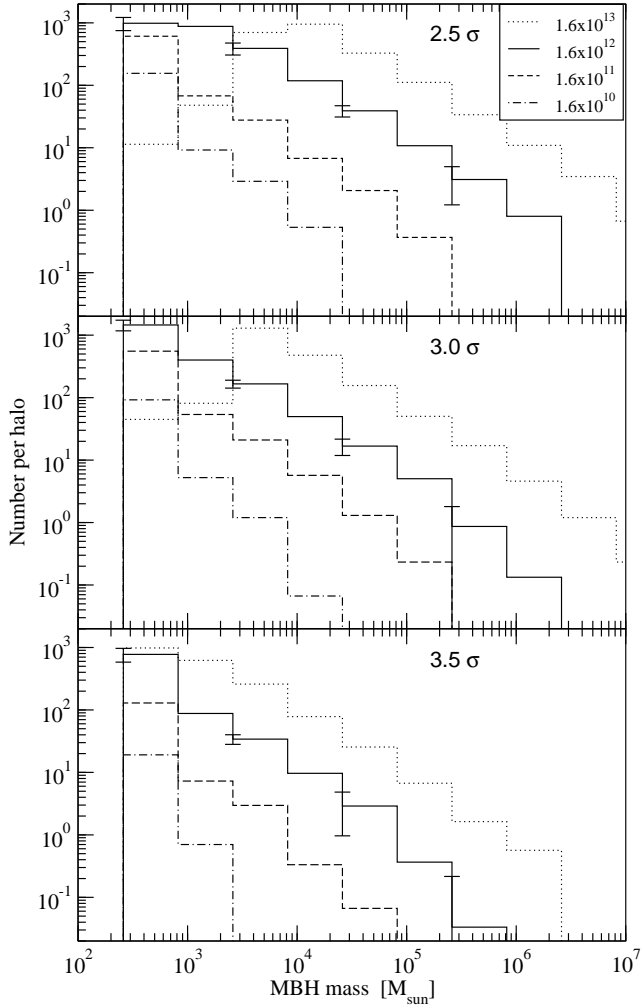


Figure 1. Abundance of all MBHs in the halo for models C, A and D (top to bottom panels) averaged over 30 trees with error bars corresponding to the standard deviation.

for the different halo masses and models is summarised in tables 2 and 3. For comparison the latter also lists the mass of the respective central SMBHs. In section 3.3 we will see that the mass of SMBHs is tightly correlated with the mass of the galactic bulge component. The table shows that the mass contained in halo MBHs is typically between two to three times larger than the mass of the central SMBH.

Together with the correlations between M_{SMBHs} and M_{bulge} and between M_{bulge} and M_{halo} this implies that a similar correlation exists between the total mass contained in MBHs and their respective halo masses. In fact, for all four halo masses this correlation is consistent with

$$\sum M_{\bullet} \propto M_{halo}^{1.0 \pm 0.03}$$

which is what we would expect, since any halo increasing its mass through the accretion of smaller haloes will also inherit all MBHs associated with the latter.

Within the standard deviation quoted we expect the number and mass abundance of MBHs particularly in the $1.6 \times 10^{12} M_{\odot}$ halo to be representative of Milky-Way-sized galaxies in currently favoured Λ CDM cosmologies.

In table 4 we have listed the average abundance of

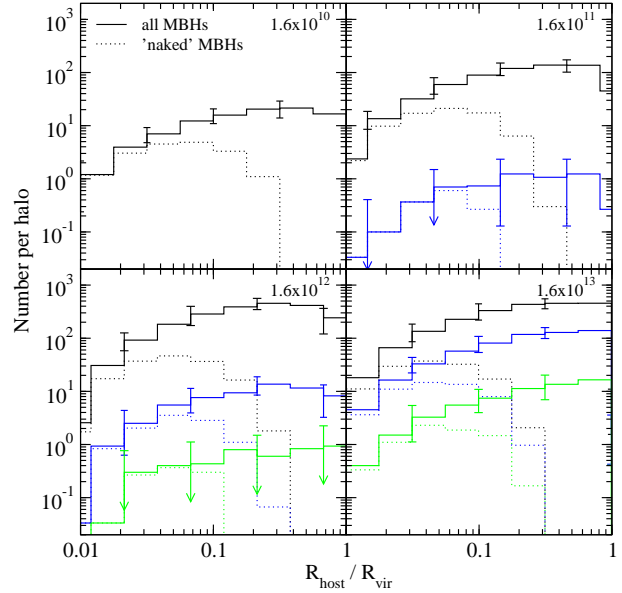


Figure 3. Radial distribution of MBHs for model A averaged over thirty trees for all four final halo masses. The contribution to the total of naked MBHs is shown by the dotted lines. In each panel the two lower sets of curves represent the radial distribution for MBHs more massive than 10^4 and $10^5 M_{\odot}$ respectively. The relative distributions of MBHs above the different mass thresholds are similar, implying that there is no obvious mass segregation.

Table 4. Abundance of MBHs in Earth-centred volumes at 8.5 kpc from the galactic centre in the Milky-Way-sized halo ($1.6 \times 10^{12} M_{\odot}$). Given are the average over thirty trees with their respective standard deviation.

	Distance from Earth Δr [kpc]		
	2.0	2.5	3.0
Model A	0.87 ± 0.94	1.7 ± 1.29	2.57 ± 1.76
Model B	0.43 ± 0.63	1.03 ± 0.96	2.00 ± 1.56
Model C	0.53 ± 0.73	1.4 ± 1.28	2.47 ± 1.87
Model D	0.23 ± 0.63	0.4 ± 0.72	0.70 ± 0.84

MBHs in a local Earth-centred volume (which we have taken as corresponding to a volume centred at 8.5 kpc from the centre of a $1.6 \times 10^{12} M_{\odot}$ halo in our simulations). Virtually all of these will be seed BHs that have not yet merged and in the absence of any growth process other than hierarchical merging their mass will be equal to that of the initial seed BHs. To the extent that the large standard deviations allow for any meaningful comparison between the models, one notable feature is the marked difference between the average number of nearby MBHs in models A and B. We already mentioned that we would not expect any significant difference in the halo (merger) dynamics and thus the final MBH abundance because the models only differ in that they start out with different MBH seed masses. However, the solar neighbourhood at 8.5 kpc from the centre is well within the radial regime where the MBH abundance is becoming increasingly dominated by naked MBHs. At distances smaller (larger) than the sun's orbit there are relatively more (less)

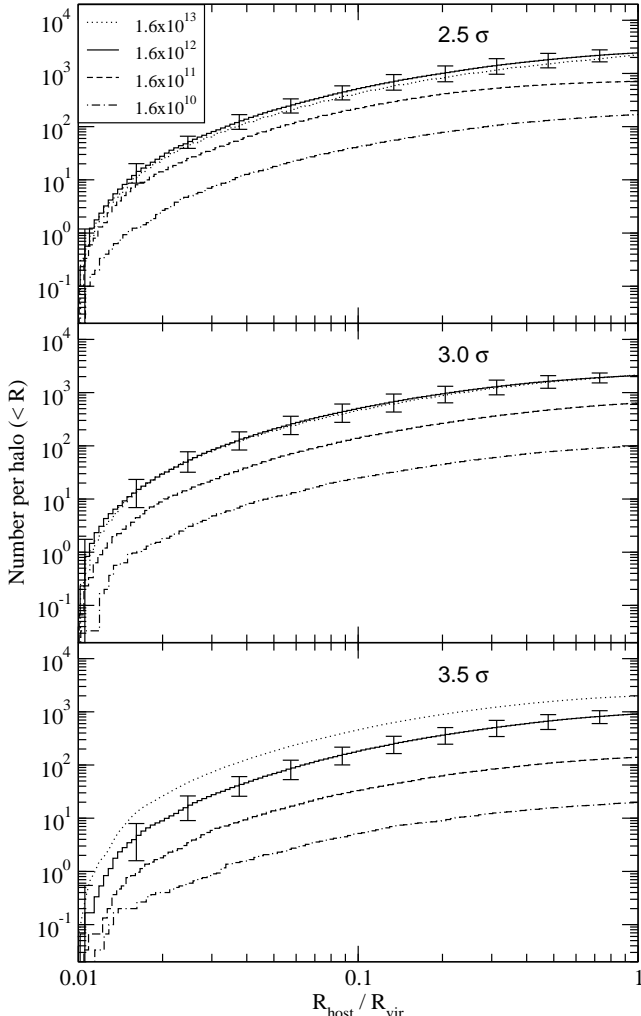


Figure 4. Number of MBHs below radius R from host centre, averaged over all trees and scaled to the respective virial radius for the individual haloes. Error bars corresponding to the standard deviation are shown for the case of the $1.6 \times 10^{12} M_{\odot}$ halo.

naked MBHs and because these are more massive they move towards the centre more quickly. This would explain why the number of nearby MBHs is consistently lower in model B for all local distances considered. Our findings for the MBH abundance in haloes are in accord with the results of another recent investigation by Volonteri, Haardt & Madau (2003, hereafter VHM03). We find that the total MBH mass density in a Milky-Way sized galactic in our model C (with a minihalo collapse threshold of 3.5σ) halo agrees to within a factor 2 with their value inferred from the density function of ‘wandering’ BHs in galactic haloes.

3.1.2 Constraints on initial MBH mass function

Figure 2 for the two different MBH seed masses gives some indication of the effect of other changes in the masses and numbers of seed MBHs in the primordial haloes.

We have seen above that the MBH mass functions are shifted along the M_{MBH} axis in proportion to the mass of the seed MBHs. This mass, however, cannot be higher than the total baryonic mass contained in the original minihaloes.

This translates into the grey shaded area shown in figure 2 and thus any mass for a single seed MBH between 260 and $1.3 \times 10^4 M_{\odot}$ will lead to a present-day MBH mass function that lies between the shaded area and the mass function corresponding to model A.

By conservation of mass ², if the primordial halo contains more than one MBH of different masses in the range $260 M_{\odot} < M_{\bullet} < 13000 M_{\odot}$ then the resulting mass function will again lie between the bottom and the top one shown, but will have a different slope. If initially one or more MBHs were present with masses lower than $260 M_{\odot}$, the present-day mass function will correspondingly extend to lower masses, but will otherwise still be limited by the shaded area. This means, that even though we had initially made a fairly specific choice for the initial MBH mass function in the primordial haloes, any general form for the MBH IMF is expected to lead to results within the limits provided by the MBH mass functions shown, if there is at least one seed MBH of $260 M_{\odot}$ or larger. This is *provided the seed MBHs form in 3σ peaks* as is the case for model A and B. Seed MBH formation in higher or lower peaks changes the overall normalisation and leads to a corresponding scaling of the mass functions. The relative range of possible mass functions should nevertheless remain reasonably well defined unless seed MBHs form in minihaloes collapsing from an extended range of peak heights and thus redshifts.

We need to stress that the above depends on the assumption that all MBHs falling to within one per cent of the virial radius merge efficiently in all haloes merging along the way to produce the final host halo.

If the only or at least most significant source of seed MBHs is that forming in minihaloes then the total mass contained in halo MBHs can be used to normalise the initial mass function of seed MBHs, to which it is related by the background cosmology. The latter determines the average merger history of haloes and thus the average number of minihaloes ending up in more massive haloes later on. Note that this is not much affected by the merger efficiency of MBHs since the present-day MBH mass function is dominated by seed MBHs that have not merged, and that contribute a similar amount to the total mass contained in halo MBHs as the few very massive MBHs that have resulted from multiple mergers of seed MBHs. This is just expressing in a different way the $N_{\bullet} \propto M_{\bullet}^{-1}$ scaling we found earlier (c.f. figure 2, which means that the total mass contributed from successive logarithmic MBH mass intervals is constant).

3.2 MBH mass accretion rates

Having established the abundance of MBHs we now look at rates at which MBHs accrete material from their surroundings. This forms the basis for any estimate of the accretion luminosities that may be detectable.

² Strictly the masses of two merging BHs are not conserved, but will be lower by a few per cent, since gravitational waves can radiate away some of the BHs’ rest mass energy. In the following we assume that this effect only changes our results by a negligible amount, although the mass loss through gravitational radiation accumulated in many mergers for some MBHs may become significant.

3.2.1 Bondi-Hoyle accretion

If we consider a MBH travelling within a uniform medium, the steady state accretion rate is given by the Bondi-Hoyle accretion rate (Bondi & Hoyle 1944; Bondi 1952)

$$\frac{dM}{dt} = \pi r_{acc}^2 \sqrt{v_\bullet^2 + c_s^2} \rho_g \quad (1)$$

Here c_s is the sound speed in the gas and ρ_g its density – both far from the MBH. v_\bullet is the velocity of the MBH and r_{acc} the accretion radius

$$r_{acc} = \frac{2GM_\bullet}{v_\bullet^2 + c_s^2} \quad (2)$$

giving an accretion rate

$$\frac{dM}{dt} = \frac{4\pi G^2 M_\bullet^2 \rho_g}{c_s^3} (1 + \beta_s^2)^{-3/2} \quad (3)$$

where we have used $\beta_s \equiv v_\bullet/c_s$ (Chisholm, Dodelson & Kolb 2002). If the MBH accretes adiabatically from a gas of pure hydrogen this is

$$\begin{aligned} \dot{M} &= 8.77 \times 10^{-12} \left(\frac{M_\bullet}{100M_\odot} \right)^2 \left(\frac{\rho_g}{10^{-24} \text{ g cm}^{-3}} \right) \\ &\times \left(\frac{c_s}{10 \text{ km s}^{-1}} \right)^{-3} (1 + \beta_s^2)^{-3/2} M_\odot \text{ yr}^{-1} \end{aligned} \quad (4)$$

It is implicit that only baryonic matter can get accreted in this way, assuming that a mechanism exists for the dissipation of thermal energy as the material falls towards the MBH. Any such process is not relevant for dark matter, which is by definition not or only weakly interacting and only gets accreted if it approaches the MBH to within a distance that is of the order of the last stable orbit of the MBH. This is much smaller – i.e. it has a much smaller ‘cross section’ – than the Bondi accretion radius and we will subsequently neglect the possibility of dark matter accretion.

In what follows we assume that while the nature of the accretion process is somewhat uncertain, the overall mass accretion rate is essentially determined by the Bondi-Hoyle formula. This implies, that we neglect the possibility that the mass accretion rate is modified e.g. by a non-negligible mass of an accretion disk that may form around the accreting MBHs.

3.2.2 Accretion environment: ISM vs. baryonic core remnants

As the MBHs orbit through the host halo they accrete matter from the host ISM. This will only be significant in regions with relatively large amounts of gas, which is the case primarily in the galactic disk and bulge.

Alternatively the MBHs may accrete from a core remnant of the satellite they were originally associated with. In our numerical procedure a satellite is considered tidally disrupted when the tidal radius becomes smaller than the scale radius of the satellite density profile. We have so far referred to MBHs embedded in such satellites as ‘naked’ MBHs. This condition is sufficient as far as the dynamical importance of the satellite is concerned, since at this stage it will have lost all but at most a few percent of its mass. However, even in these systems a core remnant close to the satellite centre

may still remain. While insignificant for the overall dynamics of the satellite the amount of baryonic matter contained in this core could still contribute significantly to the accretion onto a MBH that is present at its centre and so boost its accretion luminosity potentially by orders of magnitude. In this case MBH accretion is independent of the conditions and relative MBH velocity in the surrounding ISM of the host halo.

To determine the mass accretion rate we still need an estimate of the gas density in the baryonic core that is essentially acting as fuel supply travelling along with the MBH. Assuming that all baryonic matter has cooled in the satellites before they are subject to tidal stripping and heating in the host the outer radius of the baryonic core assumed spherical is $r_b \sim 0.1r_{vir}$ where r_{vir} is the virial radius of the unstripped satellite halo of mass M_{vir} . If all baryons are in the form of gas and the baryon fraction in the satellite is cosmological, i.e. $M_b = (\Omega_b/\Omega_m) M_{vir}$, then the mean gas density is

$$\rho_g = \frac{3M_b}{4\pi r_b^3} = \frac{1}{0.001} \frac{\Omega_b}{\Omega_m} \frac{3M_{vir}}{4\pi r_{vir}^3} \approx 2.39 \times 10^2 \frac{\Omega_b}{\Omega_m} \frac{M_{vir}}{r_{vir}^3} \quad (5)$$

Substituting this into equation (12) and using $c_s \approx 10 \text{ km s}^{-1}$ for ISM at 10^4 Kelvin we can determine the mass accretion rate

$$\begin{aligned} \dot{m} &\approx 6.25 \times 10^{-8} \left(\frac{M_{MBH}}{M_\odot} \right) \frac{\Omega_b}{\Omega_m} \left(\frac{M_{vir}}{10^5 M_\odot} \right) \\ &\times \left(\frac{r_{vir}}{1 \text{ kpc}} \right)^{-3} \left(\frac{c_s}{10 \text{ km s}^{-1}} \right)^{-3} \end{aligned} \quad (6)$$

and thus the luminosity. Here \dot{m} is the mass accretion rate in units of the Eddington accretion rate

$$\dot{m} \equiv \frac{\dot{M}c^2}{L_E} = 1.53 \left(\frac{\dot{M}}{10^{17} \text{ g s}^{-1}} \right) \left(\frac{M_\bullet}{M_\odot} \right)^{-1} \quad (7)$$

3.2.3 Distribution of mass accretion rates

In figure 5 we have plotted the number of MBHs vs their respective mass accretion rates for ISM as well as baryonic core accretion. The plot serves primarily to highlight the vast difference in accretion rates for the two models. In general the accretion rates for ISM accretion are lower than that for baryonic core accretion by some 7 - 10 orders of magnitude! We can see that for the case of ISM accretion the maximum accretion rate does not exceed $\sim 10^{-7}$ of the Eddington value. It seems then that ISM accretion in the context of our model is completely insignificant. There are two reasons for this. Firstly, MBHs are distributed across the halo as we have seen above, with the number of MBHs in the disk and bulge small and certainly very much lower than that of stellar mass BHs. Secondly, even in the disk and bulge the actual density of accretable gas is too low especially at late times. In our analysis of the observable signatures of accreting MBHs we therefore mainly focus on baryonic core accretion for which we get consistently larger accretion rates.

For model A we show in figure 6 the average distribution of mass accretion rates of MBHs for various redshifts in a halo that grows to mass $1.6 \times 10^{12} M_\odot$ at $z = 0$. We see that for increasing redshift the lower end of the range of accretion rates moves towards higher values. The reason for

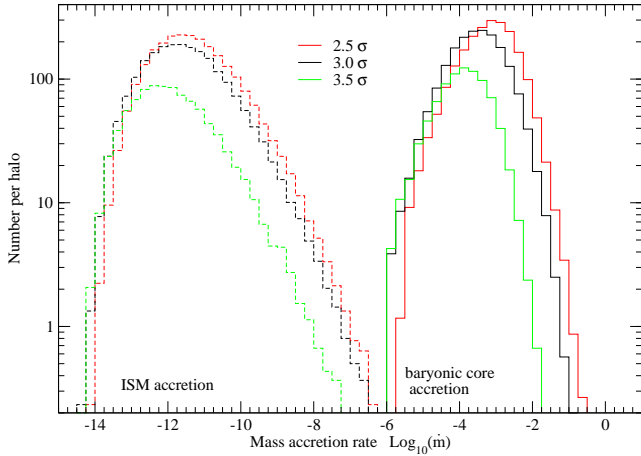


Figure 5. Abundance of accretion rates for MBHs in a Milky Way sized halo for models A, C and D. The curves on the left correspond to ISM accretion, the ones on the right to baryonic core accretion.

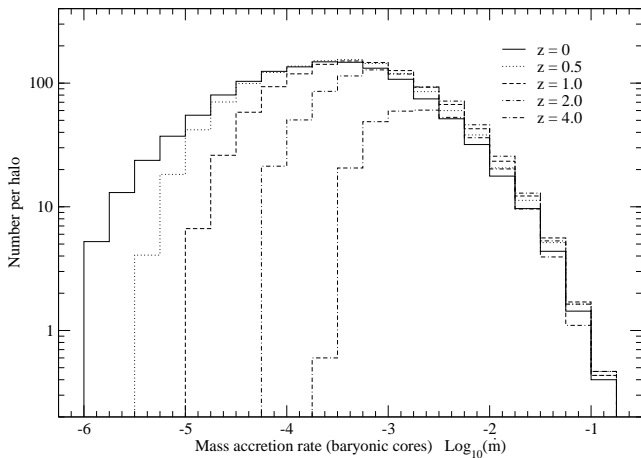


Figure 6. Redshift dependence of baryonic core accretion in model A and a final halo mass of $1.6 \times 10^{12} M_{\odot}$. At late times the host virial radius becomes largest. The resulting inclusion of low mass haloes with correspondingly small MBHs leads to an increase of objects with low accretion rates. (This particular plot is based on a different set of simulations which does, however, use the same key cosmological parameters.)

this is that at late times, as the host virial radius becomes larger, more satellites are being incorporated in the outer parts of the host. Most of these will be small satellites with seed mass MBHs

It is also interesting to note that the maximum accretion rate in all cases does not exceed a value of more than about 10 % of the Eddington mass accretion rate. Assuming that the maximum accretion rates have never been larger than this it is obvious that gas accretion from baryonic cores for most MBHs does not lead to significant mass increase over a Hubble time. This is shown in figure 7 where we have plotted the accretion rates in Eddington units for all final halo masses in models A, C and D. In particular we have marked various fractions of MBHs that accrete at rates such that their mass would increase by a factor 2, 10 and 100 respectively within a Hubble time provided the rate stays

constant. Except for the most massive haloes not more than about 10 percent of MBHs accretes even enough to double their mass, while in all cases no more than about 20 percent grow in mass by more than a factor of 100. The factor 2 mass increase is of special importance: In the most conservative baryonic core accretion scenario we would expect an MBH to be embedded in a core that contains an amount of material at least of the order of the initial MBH mass. This is to say the MBH holds on to the material within its initial range of influence. If this applied to all MBHs we would have to discount any MBHs accreting at a rate higher than needed to double their mass within a Hubble time - call this $\dot{m}_{2\times}$, since they would have consumed their core by now. We will not undertake a selection of presently accreting MBHs on the basis of this criterion, because accretion rates for most MBHs are clearly below $\dot{m}_{2\times}$. We also assume that a baryonic core is significantly more massive than the mass of the MBH. This is plausible as the baryonic component has condensed at the centre of haloes and thus is much less affected by any tidal stripping of the outer parts of the halo which are dominated by dark matter.

In the context of our baryonic core accretion model realistic accretion rates are likely to be significantly lower, especially at low redshift, when a lot of gas has already been used up in star formation - an effect that we have not accounted for in our simulations.

The distribution of data points for the most massive haloes in figure 7 can be fit by a power law

$$\dot{m} \propto M_{\bullet}^{0.68 \pm 0.02} \Rightarrow \dot{M} \propto M_{\bullet}^{1.68 \pm 0.02} \quad (8)$$

i.e. the most massive MBHs are also those accreting at the highest rates in general. Due to the scatter in the plots some of the largest dimensionless accretion rates do actually occur for MBHs that are one or two orders of magnitude lighter than the most massive ones. However, the largest physical accretion rates³ and thus accretion luminosities are indeed those of the most massive MBHs.

3.3 Abundance and mass of SMBHs

MBHs that move at distances from the centre less than 1 % of the host virial radius are considered as having fallen to the centre (c.f. section 2.3). In line with the assumption of efficient merging the mass of these infalling MBHs is simply added to the mass of a single SMBH growing at the centre.

3.3.1 SMBH from hierarchical merging of remnant MBHs

Figure 8 shows the relation between the mass of the galactic bulge and the central SMBH if the latter grows purely through mergers of smaller MBH. The solid line represents the linear relationship between SMBH and bulge mass as determined from observations. To determine this we have used the MBH mass - bulge luminosity relation based on more recent compilation of data (Kormendy & Gebhardt 2001)

$$\left(\frac{M_{\bullet}}{M_{\odot}} \right) = 1.24 \times 10^{-3} \left(\frac{L}{L_{B,\odot}} \right)^{1.08} \quad (9)$$

³ These are not scaled to the MBH mass as is the case for the dimensionless accretion rates.

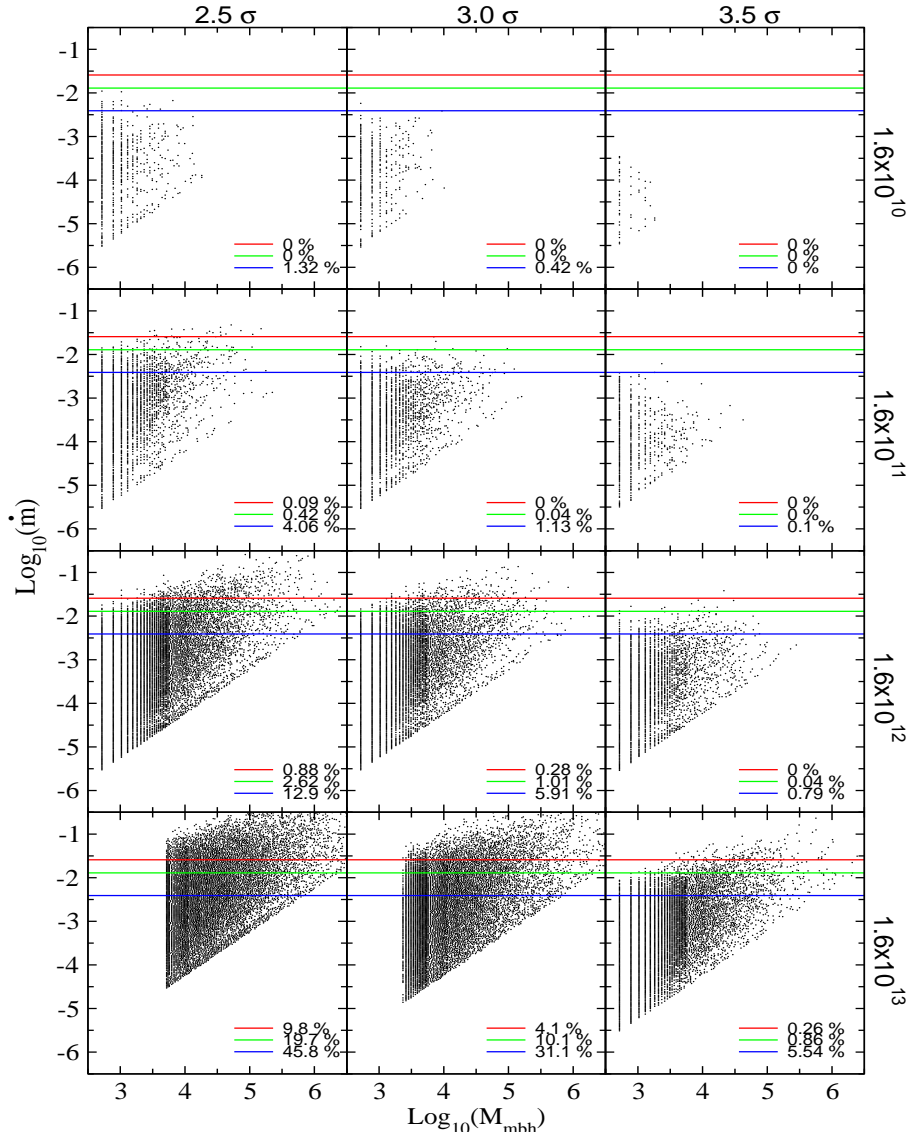


Figure 7. Dimensionless baryonic core accretion rates in Eddington units vs. MBH mass for all final halo masses in models C, A and D (from left to right). The results shown are for all 30 trees. In each panel the horizontal lines from top to bottom denote the accretion rates above which the MBH mass would grow by at least a factor 100, 10 and 2 respectively, within a Hubble time, provided the accretion rate stays constant. The percent figures show the fraction of MBHs with accretion rates higher than the respective cut-offs.

where M_\bullet denotes the mass of the SMBH. We have then combined this with the mass to light ratio determined by Magorrian et al. (1998)

$$\left(\frac{M_\bullet}{M_\odot}\right) = 0.33 \pm 0.11 \left(\frac{L}{L_\odot}\right)^{1.18 \pm 0.03} \quad (10)$$

We also assumed that the B band luminosity is approximately the same as the bolometric luminosity $L_{B,\odot} \approx L_\odot$. The observed relation places an upper limit on the allowed masses of seed MBHs and peak heights in the initial density field. The normalisation of the $M_\bullet - M_{bulge}$ mass relation in figure 8 is primarily a function of the mass density of MBHs which, in the absence of accretion, is defined by the number and mass of the seed MBHs in our model. For model B no significant gas accretion is required to match the observed relation and even for models A and C accretion would only be required to increase the SMBH mass by less than a factor

of 10. Only in model D (also the fiducial model of VHM03) gas would actually have to raise the SMBH mass by about a factor 100.

The slope of the observed relation, $M_\bullet \propto M_{bulge}^{0.92 \pm 0.02}$ is very similar to those of the best fits to our data. All the best fits in figure 8 have $M_\bullet \propto M_{bulge}^{0.90 \pm 0.01}$, except for the model with 2.5σ , $M_{\bullet,seed} = 260 M_\odot$, for which we get $M_\bullet \propto M_{bulge}^{0.93 \pm 0.01}$. This agreement is surprising, especially since one would intuitively expect a simple linear relation between M_\bullet and M_{bulge} in our merger only scenario. On the other hand, this close agreement raises the question of whether the observed slope is primarily a relic of the hierarchical merger process rather than the result of accretion processes.

To the extent that gas accretion occurs it does not alter the slope, i.e. all SMBHs grow through gas accretion by the same factor. At first sight this would seem to be in contradiction to the result for halo MBHs that more massive MBHs

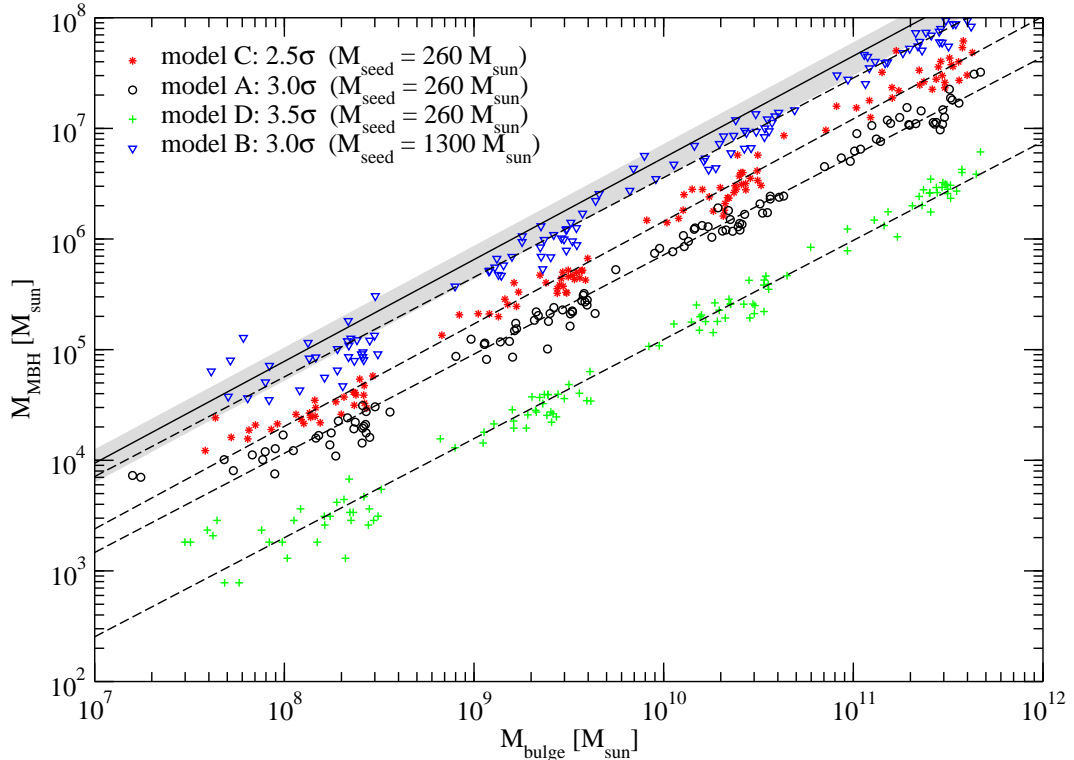


Figure 8. Central SMBH masses vs. bulge mass for all seed MBH masses and peak heights considered (models A – D). For each combination the data for all corresponding final halo masses have been grouped together. Dashed lines represent the best fits to the data. The solid line and shaded area are the $M_{SMBH} - M_{bulge}$ relation and associated error from Magorrian et al. 1998.

systematically accrete at higher rates (c.f. figure 7). We can resolve this in the same way as for halo MBHs: At low redshifts a significant if not the largest amount of accretable gas may have already been consumed in star formation.

For the SMBHs our results are also consistent with that of VHM03. For model A, for instance, we found the mass of a central SMBH in a Milky-Way sized halo to be $1.5 \times 10^6 M_\odot$. Accounting for the difference in seed MBH masses used this agrees with the central SMBH mass of $\sim 1 \times 10^6 M_\odot$ for a halo of mass $1.6 \times 10^{12} M_\odot$ with $\sigma \sim 155 \text{ kms}^{-1}$ as implied by their $M_\bullet - \sigma$ relation (with no gas accretion). This also coincides with the mass determined for the SMBH in the Milky Way, although the Milky Way SMBH is known to lie significantly below the observed $M_\bullet - \sigma$ relation.

However, our slightly non-linear $M_\bullet - M_{bulge}$ correlation corresponds to a $M_\bullet - \sigma$ relation whose logarithmic slope (~ 4.0) does not match the much flatter one they determined (~ 2.9) for 3σ collapse and no gas accretion. We believe this to be possibly a result of the different assumptions made about the MBH merger process. In particular the inclusion of triple BH interactions and sling-shot ejections by VHM03 would probably lead to even lower central SMBH masses in our analysis.

3.3.2 SMBH growth from gas accretion

A number of studies (Soltan 1982; Yu & Tremaine 2002) suggest that the present day SMBH mass density is consistent with the amount of gas accreted during the optically bright QSO phase. If this is the case then our model B is

probably ruled out as it only requires a mass increase of order unity to match the observed abundance of SMBHs today. Models A, C and D would not be affected as gas accretion would still be needed to increase the SMBH masses by at least a factor 3.

On the other hand gas accretion (during the QSO phase) alone cannot explain growth from stellar mass BHs to the most massive SMBHs ($\geq 10^9 M_\odot$). Even if stellar mass BHs are accreting at the Eddington limit, the QSO phase would not last long enough for the BHs to grow sufficiently.

If BHs accrete at the Eddington limit their mass doubling time is given by the Salpeter time scale,

$$t_{salp} \sim \frac{\eta M c^2}{L_{edd}} = \frac{\eta \sigma_t c}{4\pi G m_p} \sim \eta 4.5 \times 10^8 \text{ yr} \quad (11)$$

The quasar epoch lasts about 10^9 years from a redshift of about $z \sim 3.5 - 1.5$ (Richstone et al. 1998). Typical QSO lifetimes are estimated to be $t_Q \sim 10^7 - 10^8$ yrs. Even if we assume that a series of major mergers has triggered individual QSOs repeatedly such that they are active through most of the QSO epoch, the BHs would only grow by a factor of order 10^6 but likely less.

Semi-analytical models of galaxy formation assume that following the QSO epoch the (S)MBHs powering quasars grew further through major mergers (Haehnelt & Kauffmann 2000). However, the latter is unlikely to have raised the (S)MBH mass by more than an order of magnitude. This means that MBHs with masses of at least $10^2 - 10^3 M_\odot$ must have been present at the beginning of the QSO epoch already. This is confirmed by the presence of luminous quasars at redshifts higher than $z \sim 6$. In fact,

the latter means that at least some SMBHs must have been in place by that time as the Universe was hardly old enough to accommodate a long enough Eddington limited gas accretion phase to explain their mass (Haiman & Loeb 2001).

Our model complements this idea. Hierarchical merging involving seed MBHs originating at $z \gtrsim 20$ can produce the number and masses of (S)MBHs needed at the onset of the QSO epoch. To test this idea we estimate the density of SMBHs with a mass of at least $10^8 M_\odot$ which we take as the mass required to power a QSO - at a redshift $z \sim 6$. Since only some fraction of QSOs are active, the number density of SMBHs has to be at least as large as the density of luminous QSOs at that redshift, which is $\sim 10^{-7} \text{ Mpc}^{-3}$ (Richstone et al. 1998). This number density corresponds to the abundance of haloes of mass $6 \times 10^{12} M_\odot$ at redshift $z = 6$ in the Λ CDM model we are working with. If we assume that the $M_\bullet - M_{bulge}$ relation in figure 8 and the $M_\bullet - M_{host}$ relation in table 3 will be the same at $z = 6$ then there is a problem: For a halo mass of $6 \times 10^{12} M_\odot$ models A and C imply a SMBH mass of 5×10^6 to $1 \times 10^7 M_\odot$. However, if we allow for gas accretion at only a fifth of the Eddington rate these SMBHs could have certainly grown by an order of magnitude by $z = 6$. We conclude then that Eddington limited gas accretion alone onto an initially stellar mass BH or even a moderate mass MBH cannot produce the number density of SMBHs required to explain QSOs at redshifts of $z \sim 6$. The need for intermediate mass seed BHs and/or some merging of MBHs/SMBHs is therefore necessary to explain the presence of the most massive SMBHs.

3.4 Effect of low merger efficiency

If the merging of MBHs does not proceed efficiently, our results presented above will be affected in two major respects. In our model the build-up of SMBHs requires the merging of MBHs at the centre of merging haloes. If merging does not occur efficiently, SMBHs would have to grow by other processes, such as gas accretion. Similarly MBHs with masses larger than the MBH seed mass would be much harder to form, i.e. the number of the most massive MBHs orbiting in haloes would be very much lower. Since the MBH accretion rates depend also on halo mass, this means that the number of MBHs with high accretion rates and accretion luminosities will be reduced, too.

Interestingly – and contradictory at first sight – less efficient merging opens up more possibilities for processes to aid the merging of MBHs. If merging is less efficient, gas accretion will have to play an even more prominent role in MBH growth. It could be argued that, if gas accretion is a generic and decisive constituent of MBH growth even at high redshifts, the resulting mass increase of MBHs would enhance the subsequent merging of MBH binaries. Secondly, less efficient merging implies that three body interactions can occur. Typically, if three or more MBHs interact, the lightest ones will be slingshot-ejected from the system, leaving behind a binary that is yet more tightly bound and will merge in a shorter time. This is the same process as for stellar dynamical interactions mentioned in section 2.3, albeit with a much higher efficiency per interaction.

In one important respect, however, a lower merger efficiency has no significant effect. We have seen above that the number of MBHs in haloes is inverse proportional to the

MBH mass. The number of halo MBHs is therefore dominated by seed MBHs, and a change in merger efficiency would not significantly affect the total number of MBHs in haloes.

4 EMISSION SIGNATURES FROM MBHS AND ASSOCIATED SATELLITES

On the basis of the accretion rates computed in the previous section we now determine the corresponding bolometric accretion luminosities. In the absence of any detailed spectral modelling, these provide at least an indication of the magnitude of expected observational signatures.

The bolometric luminosity L_{bol} is directly proportional to the physical mass accretion rate times the radiative efficiency parameter η

$$\begin{aligned} L_{bol} &= \eta \frac{dM}{dt} c^2 \\ &= \eta 5 \times 10^{35} \left(\frac{M_\bullet}{100 M_\odot} \right)^2 \left(\frac{\rho_g}{10^{-24} \text{ g cm}^{-3}} \right) \\ &\quad \times \left(\frac{c_s}{10 \text{ km s}^{-1}} \right)^{-3} (1 + \beta_s^2)^{-3/2} \text{ erg s}^{-1} \end{aligned} \quad (12)$$

and c is the speed of light. η can reach maximum values of $\eta_{max} \approx 0.06$ for non-rotating black holes and up to $\eta_{max} \approx 0.4$ for maximally rotating black holes (Shapiro & Teukolsky 1983), if a mechanism for the effective dissipation of energy exists. This mechanism is provided for by the viscosity of matter in the accretion flow.

4.1 Bolometric luminosity for accretion from the host ISM

The effect of ISM accretion and the resulting emission has previously been investigated analytically for stellar mass BHs in our galaxy that are the remnants of ordinary stellar evolution (Fujita et al. 1998). For MBHs larger luminosities are expected, particularly when they travel within or are crossing the galactic disk and bulge regions or in molecular clouds, as more gas is available. But even in less dense regions of the inter stellar medium (ISM) MBHs could generate sizable luminosities if they travel at low velocities and have a correspondingly larger accretion radius.

In particular ISM turbulence can establish a geometrically thin accretion disk around the MBH with an associated radiative efficiency that can reach the maximum values mentioned above. For our computations we have adopted a ‘standard’ thin disk radiative efficiency of $\eta_{td} = 0.1$, and used the ISM accretion rates determined in the last section.

The resulting bolometric luminosity function for the MBHs in individual haloes is shown in the top panel of figure 9. This also shows the contribution of MBHs above various mass thresholds.

In the last section we have seen that ISM accretion occurs at a very much smaller rate than that from baryonic cores and the question is how low the resulting accretion luminosity would be. In fact from figure 9 it becomes clear that MBHs accreting from the host ISM have luminosities so low that it appears very difficult to detect them let alone identify

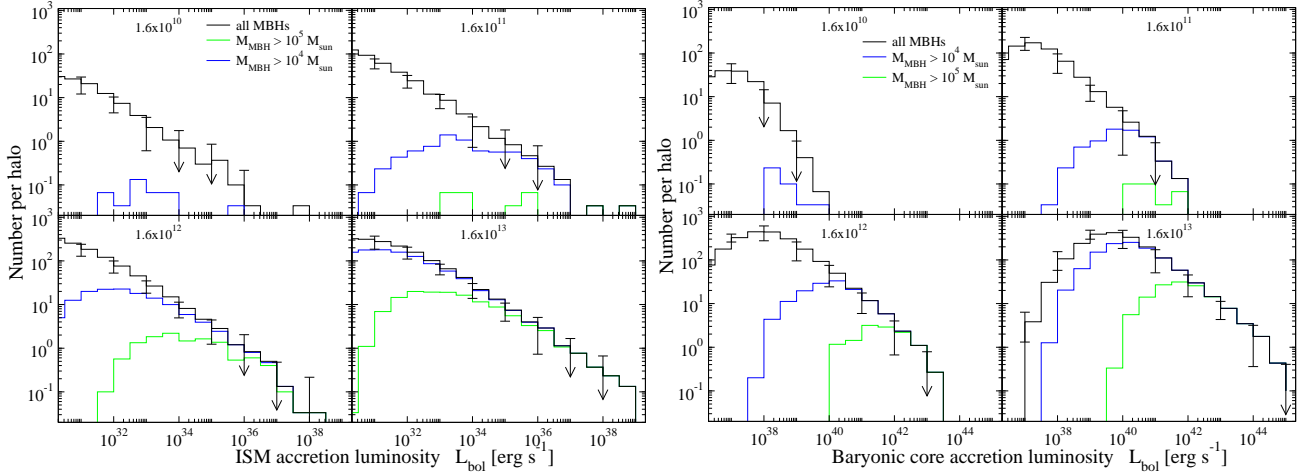


Figure 9. Bolometric luminosity functions for model C in the case of accretion from the host ISM (top panel) and from baryonic cores (bottom panel). Results are shown for all final halo masses and MBH mass cuts as shown.

them as MBHs. It might still be possible to derive statistical constraints were the number of objects large enough⁴. For instance in an inhomogeneous ISM, that we have not accounted for in our model, BHs travelling through dense regions in the galactic disk or bulge would emit at significantly larger luminosities. A MBH accreting within a dense cloud that has a density a factor 10 higher than the average, say, would see its luminosity boosted by about the same factor (c.f. eq. 12). By conservation of mass, however, these clouds would only fill $\lesssim 1/10$ of the ISM volume. If we have 10 MBHs uniformly distributed across the host ISM and accreting at $10^{36} \text{ erg s}^{-1}$ only at most one would end up in a cloud with ten times larger density at any one time. However, in our case the numbers of MBHs are just too low for this process to be significant.

Figure 9 shows the result for model C, which serves to illustrate that even for the model that produces the highest number of large MBHs in the most massive haloes, the number of MBHs accreting at bolometric luminosities larger than $\sim 10^{37} \text{ erg s}^{-1}$ is insignificant. The main cause for these very low ISM accretion rates is that most MBHs orbit at distances larger than the light radius of the galaxy, which means that even if accretion luminosities were very large in the disk and bulge we would still only observe very few sources there.

Regarding this last point, baryonic core accretion also offers the advantage that it is essentially independent of the structure and geometry of the host ISM.

4.2 Bolometric luminosity for accretion from baryonic core remnants

In the previous section we argued that MBHs accrete from a disk assuming that the net specific angular momentum created in the surrounding host ISM through turbulence is large enough.

⁴ See e.g. Fujita et al. (1998) who consider of the order of $10^6 \text{ BHs kpc}^{-3}$ (Fujita et al. 1998)

For accretion from baryonic cores the required net angular momentum comes for the largest part from the angular momentum of the original satellite. Although the outer parts of satellites may have been stripped and their angular momentum deposited in the host halo, the cores will preserve most of their angular momentum. In this sense we can view these MBH - baryonic core systems as the engines of mini-AGN stripped of their halo/galaxy within which they originally resided.

Based on the baryonic mass accretion rates obtained in the previous section and using the 10 % standard thin disk efficiency, we obtain a differential MBH bolometric luminosity function which is shown in the right panel of figure 9 for model C. $\beta_s = 0$ in this case as the MBHs have no relative motion with respect to the baryonic cores from which they accrete. Figure 10 shows what we call the projected bolometric luminosity function, that is of all sources within a halo, whose lines-of-sight (LOS) fall within some distance from the centre normal to the LOS. Overall we see that the accretion luminosities are much higher than for the ISM accretion case. They attain values larger than $10^{40} \text{ erg s}^{-1}$, although luminosities are somewhat lower for models A and D with their lower MBH mass density.

The luminosity functions for the two most massive haloes exhibit a logarithmic slope in the declining part of the function.

$$N_{\bullet} \propto L_{bol}^{-0.6 \pm 0.02} \quad (13)$$

Also from equation 8

$$L_{bol} \propto \dot{M} \propto M_{\bullet}^{1.68 \pm 0.02} \quad (14)$$

Comparing with equation 12 this implies a non-trivial scaling relation between M_{\bullet} and the satellite gas density

$$M_{\bullet} \propto \rho_g^{3.13 \pm 0.2} \quad (15)$$

Across all luminosities the largest fraction of the sources is distributed throughout the host. Many of the brightest ones are in fact at distances larger than 10 percent of the host virial radius R_{vir} . The numbers of sources in the bulge and the disk are similar and relatively low. Inside our galaxy

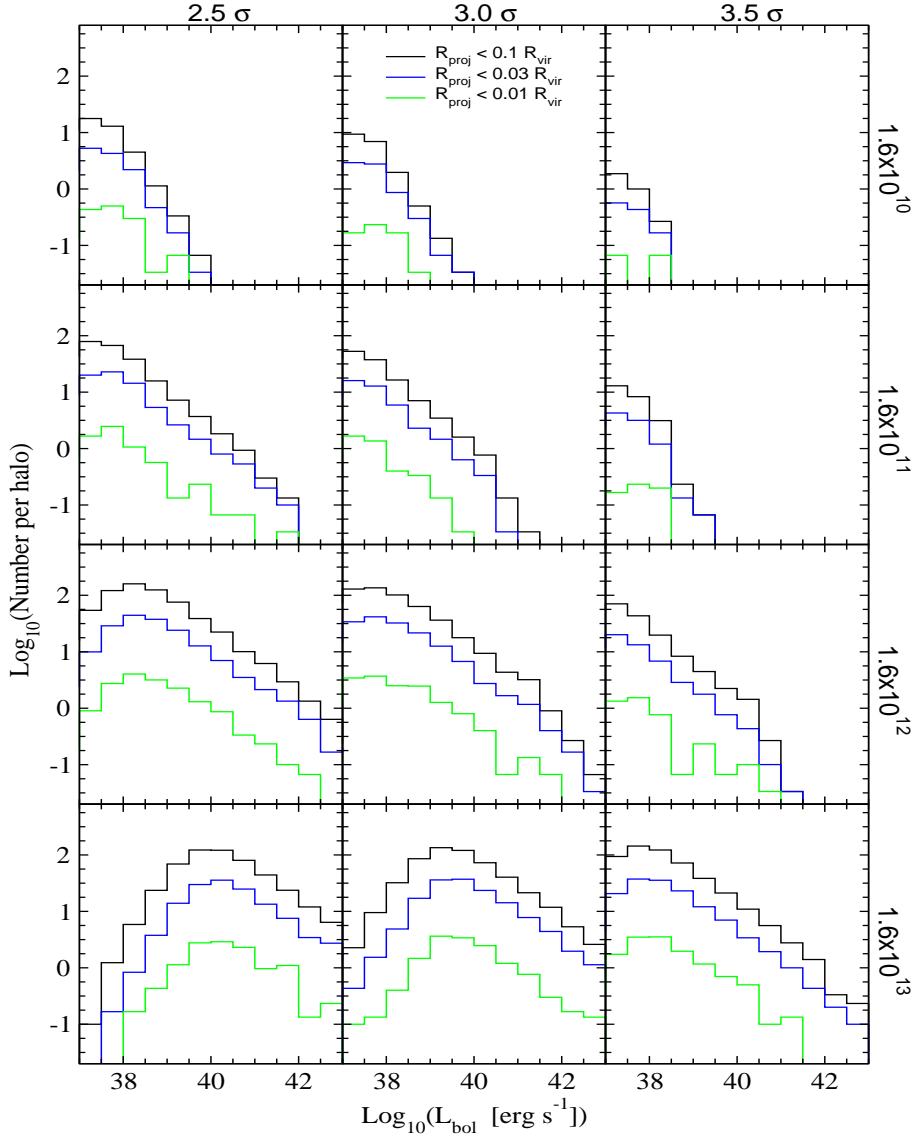


Figure 10. Bolometric luminosity of MBHs accreting from baryonic cores for models C, A and D (left to right panels). Shown are the sources whose line of sight falls within some projected distance from the host centre.

most of the sources should therefore not be affected by strong absorption in the disk and bulge. For other galaxies, however, these problems remain for those MBHs whose line-of-sight passes close to the central region of the galaxy within which they are located.

4.3 Dark matter spikes and annihilations

Accretion plays an important role in SMBH growth, as inferred both from the preceding discussion of the SMBH-spheroid correlation and independently from the coincidence between black hole mass density and the integrated, accretion-fed, luminosity density of quasars. If the MBH grew adiabatically, for example via gas accretion onto a seed MBH, a spike develops in the CDM density profile within the region of gravitational influence of the MBH, $R \sim GM_{MBH}/\sigma^2$, where σ is the minihalo central velocity dispersion. The cusp profile steepens from $\rho \propto r^{-\gamma}$ to $\rho \propto r^{-\gamma'}$,

with $\gamma' = \frac{9-2\gamma}{4-\gamma}$ (Gondolo & Silk 1999). Of course the central SMBH did form by mergers, and such a spike would have been disrupted (Ullio, Zhao & Kamionkowski (2001)). However most of the surrounding MBHs have not suffered a recent merger, within the age of the spheroid, and the CDM spikes would have survived or been renewed as the MBH grew by accretion.

It is generally believed that the CDM consists of neutralinos, the favoured stable massive MSSM (Minimal Super Symmetric Model) candidate whose relic density was determined by the annihilation rate in the early universe at the epoch of thermal freeze-out. These neutralinos continue to annihilate today in the dark halos, albeit at very slow rates that in principle can be calculated by spanning MSSM parameter space once the relic abundance is specified. The CDM spikes result in a greatly enhanced annihilation rate that can yield potentially detectable byproducts such as high energy gamma rays, positrons and antiprotons. Indeed it has

even been suggested that an unidentified EGRET source in the direction of the galactic centre might be due to such a spike (Bertone et al. 2002). One motivation for this suggestion was that the EGRET spectrum is too hard to be consistent with hadronic interactions by cosmic rays and is consistent with an annihilation origin.

However, a reanalysis of the EGRET data has led to a new positional identification of the GC EGRET source not with SagA* but with a nearby massive star cluster (the Arches) (Hooper & Dingus 2002). Also, the unexpected presence of massive stars with plunging orbits in the vicinity of the SMBH associated with SagA* (Ghez et al. 2003) has been attributed to the infall of massive stars under the gravitational influence of a IMBH (a MBH of mass $10^3 - 10^4 M_\odot$) that represents the robust core of a star cluster able to survive tidal disruption and end up in the vicinity of SagA* (Hansen & Milosavljević). We conjecture that this IMBH and others are relics of disrupted minihalos and their baryonic cores, which still contain CDM spikes. One might therefore be seeing off-centre gamma ray sources associated with spike annihilations. Indeed other unidentified EGRET sources might also be due to relic annihilation spikes. The predicted *gamma*-ray flux is uncertain by several orders of magnitude due to uncertainty in the the initial CDM cusp profile prior to spike formation and to the MSSM parameter space. One could therefore be seeing MBHs at 10 kpc distance of mass well below $10^6 M_\odot$, and possibly down to $10^3 M_\odot$. Predicted spectra should be hard, possibly extending to several 100 GeV, since the expected neutralino mass range is approximately 50 GeV–2TeV.

5 SUMMARY AND CONCLUSIONS

We have used a semi-analytical approach to track the merger history of massive black holes and their associated dark matter haloes, as well as the subsequent dynamical evolution of the MBHs within the new merged halo. In particular we have looked at the possibility that MBHs that are the remnants of massive population III stars, forming in low mass haloes at redshifts $z \sim 20 - 30$, could hierarchically build up to contribute to the present-day abundance of central galactic SMBHs. If this is the case then a number of remnant MBHs are expected to orbit inside galactic haloes. We expect our results to be representative for Λ CDM cosmological models.

Our results can be summarised as follows:

- For a range of models that consider different seed MBH masses as well as various collapse thresholds and redshifts for minihaloes we have determined the abundance of remnant MBHs in present day galactic haloes. As a result we expect of the order of a 1000 MBHs mostly with masses near the initial seed mass at the lower end and a few as massive as 10^4 to $10^5 M_\odot$.
- We have considered two accretion scenarios for the MBHs. For the case that MBHs accrete from the host ISM we found that the resulting accretion rates are too small for any related observational signatures to be significant. Instead accretion from baryonic core remnants of the satellite haloes that MBHs are/were originally associated with yields much larger accretion rates. Assuming a radiative efficiency of 10%, a few MBHs within the visible extent of a galaxy

would be expected to display bolometric accretion luminosities in excess of $10^{41} \text{ erg s}^{-1}$. This appears inconsistent with observations of ultraluminous off-centre X-ray sources that have been detected in a number of galaxies (see e.g. Colbert & Mushotzky 1999). However, since most MBHs in our model accrete at only a fraction of the Eddington rate, this raises the possibility of radiatively inefficient accretion flows with correspondingly lower accretion luminosities. This option will be explored further in a subsequent paper.

- The slope of the $M_{\text{SMBH}} - M_{\text{bulge}}$ relationship in our model almost exactly matches that of observations, perhaps indicating that MBH merging really is a generic part of SMBH growth. Depending on the formation redshift of minihaloes and assumed mass of seed MBHs, however, various amounts of gas accretion are required to also match the normalisation of the observed relation.
- Our model complements gas accretion based growth models for MBHs. It produces an appropriate number of MBHs and SMBH at high redshifts without which gas accretion alone could not explain the most massive SMBHs today as well as the presence of QSOs at redshifts of 6.

Our numerical results depend on a number of parameters that are not yet well constrained, notably the primordial initial mass function of metal poor stars forming inside minihaloes. However, we have shown that, particularly for the abundance of MBHs in the halo, our results hold qualitatively for a wide range of different primordial IMFs, provided stars turn into MBHs of similar mass.

If the halo MBHs could be uniquely identified by their X-ray emission or otherwise, then within the context of our model they could also be used to tag (remnants of) substructure orbiting in a galactic halo. In this way they would complement counts and location of dwarfs and star clusters as measures of substructure in the galaxy and the halo.

Our results for the growth and present-day mass of the central SMBHs do depend sensitively on how efficiently MBHs merge at the host centre. Here we have taken the view that during major mergers any MBHs orbiting within the core region of the host will be quickly dragged towards the central SMBH, aided by the massive inflow of gas. Inspiral of the MBH by dynamical friction could further be boosted by the presence of a high density baryonic and dark matter core that remains associated with the MBH and could thus potentially increase the mass by orders of magnitude.

ACKNOWLEDGMENTS

The authors wish to thank R. Bandyopadhyay, G. Bryan, J. Magorrian and H.-W. Rix for helpful discussions. RRI acknowledges support from Oxford University and St Cross College, Oxford. JET acknowledges support from the Leverhulme Trust.

REFERENCES

Abel T., Bryan G.L., Norman M.L., 2000, ApJ, 540, 39
 Adams F.C., Graff D.S., Richstone D.O., 2001, ApJ, 551, L31
 Armitage P.J., Natarajan P., 2002, ApJ, 567, L9
 Barnes J.E., 2002, MNRAS, 333, 481
 Barnes J.E., Hernquist L., 1996, ApJ, 471, 115

Begelman M.C., Blandford R.D., Rees M.J., Yu Q., Tremaine S., 2002, MNRAS, 335, 965
 1980, Nature, 287, 307

Bertone G., Sigl G., Silk J., 2002, MNRAS, 337, 98

Bondi H., Hoyle F., 1944, MNRAS, 104, 273

Bondi H., 1952, MNRAS, 112, 195

Bromm V., Coppi P.S., Larson R.B., 2002, ApJ, 564, 23

Chisholm J.R., Dodelson S., Kolb E.W., ApJ submitted,
 preprint (astro-ph/0205138)

Colbert E.J.M., Mushotzky R.F., 1999, ApJ, 519, 89

Ferrarese L., 2002, ApJ, 578, 90

Fujita Y., Inoue S., Nakamura T., Manmoto T., Nakamura K.E., 1998, ApJ, 495, L85

Fuller T.M., Couchman H.M.P., 2000, ApJ, 544, 6

Gebhardt K., et al., 2000, ApJ, 543, L5

Ghez A.M., Salim S., Hornstein S.D., Tanner A., Morris M., Becklin E.E., Duchene G., ApJ submitted,
 preprint (astro-ph/0306130)

Gondolo P., Silk J., 1999, Phys. Rev. Lett., 83, 1719

Gould A., Rix, H.-W., 2000, ApJ, 532, L29

Graham A.W., Erwin P., Caon N., Trujillo I., 2001, ApJ, 563, L11

Haehnelt M.G., Kauffmann G., 2000, MNRAS, 318, L35

Haiman Z., Loeb A., 2001, ApJ, 552, 549

Hansen B., Milosavljević M., ApJ submitted,
 preprint (astro-ph/0306074)

Heger A., Woosley S., Baraffe I., Abel T., 2002, Lighthouses of the Universe: The Most Luminous Celestial Objects and Their Use for Cosmology Proceedings of the MPA/ESO/, p. 369, 369

Hooper D., Dingus B., in 34th COSPAR Scientific Assembly of the Second World Space Congress Houston, TX, USA, 10-19 October 2002, preprint (astro-ph/0212509)

Hutchings R.M., Santoro F., Thomas P.A., Couchman H.M.P., 2002, MNRAS, 330, 927

Islam R.R., Taylor J.E., Silk J., 2003, MNRAS, 340, 647

Kormendy J & Gebhardt K. (KG01), 2001, in eds. Martel & Wheeler, Proc. AIP Symp. 586, XX Texas Symposium on Relativistic Astrophysics, New York: Am. Inst. Phys., p. 363

Laor A., 2001, ApJ, 553, 667

Machacek M.E., Bryan G.L., Abel T., 2001, ApJ, 548, 509

Madau P., Rees M.J., 2001, ApJ, 551, L27

Magorrian J., et al. (Mag98), 1998, Astron. J., 115, 2285

Menou K., Haiman Z., Narayan V.K., 2001, ApJ, 558, 535

Merritt D., Ferrarese L., 2001, MNRAS, 320, L30

Merritt D., Poon M.Y., preprint (astro-ph/0302296), (2003)

Milosavljević M., Merritt D., 2001, ApJ, 563, 34

Moore B., Quinn T., Governato F., Stadel J., et al., 1999, MNRAS, 310, 1147

Naab T., Burkert A., 2001, ASP Conf. Ser. 249: The Central Kiloparsec of Starbursts and AGN: The La Palma Connection, p. 735

Omukai K., Palla F., 2001, ApJ, 561, L55

Quinlan G.D., 1996, NewA, 1, 35

Richstone D., et al., 1998, Nature, 395, A14

Ripamonti E., Haardt F., Ferrara A., Colpi M., 2002, MNRAS, 334, 401

Schneider R., Ferrara A., Natarajan P., Omukai K., 2002, ApJ, 571, 30

Shapiro S.L. & Teukolsky S.A., "Black Holes, White Dwarfs and Neutron Stars", Wiley 1983

Silk J., Rees M.J., 1998, A&A, 331, L1

Soltan A., 1982, MNRAS, 200, 115

Somerville R.S., Kolatt T.S., 1999, MNRAS, 305, 1

Taylor J.E., Babul A., 2001, ApJ, 559, 716

Taylor J.E., Babul A., preprint (astro-ph/0301612) (2003)

Tegmark M., Silk J., Rees M.J., Blanchard A., Abel T., Palla F., 1997, ApJ, 474, 1

Ullio P., Zhao H., Kamionkowski M., 2001, Phys. Rev. D64, 43504

Volonteri M., Haardt F., Madau P., 2003, ApJ, 582, 559